

Theoretical study of orbital torque: Dependence on ferromagnet species and nonmagnetic layer thickness

Daegeun Jo^{1,2, a)} and Peter M. Oppeneer^{1,2, b)}

¹⁾Department of Physics and Astronomy, Uppsala University, P.O. Box 516, SE-75120 Uppsala, Sweden

²⁾Wallenberg Initiative Materials Science for Sustainability, Uppsala University, SE-75120 Uppsala, Sweden

(Dated: 17 November 2025)

The manipulation of magnetization in ferromagnetic metals (FMs) through orbital torque (OT) has emerged as a promising route for energy-efficient magnetic devices without relying on heavy metals. While Ti and Cu are among the most extensively studied light nonmagnetic metals (NMs) for OT devices, theoretical calculations of the resulting torque have remained limited. Here, we present a systematic and quantitative theoretical study of current-induced torques in Ti/FM and Cu/FM (FM = Co, Ni) bilayers using semi-realistic tight-binding models derived from *ab initio* electronic structures. We find that the torque in Ti/FM is larger for Ni than for Co, but this trend does not necessarily hold in Cu/FM, revealing that the FM dependence of OT is not universal but varies with the orbital current source. Moreover, the dependence of OT on NM thickness clearly indicates its NM bulk origin in both Ti- and Cu-based systems. Notwithstanding, the quantitative characteristics of OT cannot be explained by a simplified picture based on the individual bulk properties of the NM or FM layers. These results provide microscopic insight and practical guidance for designing light-metal-based orbitronic devices.

I. INTRODUCTION

The manipulation of magnetization by electrical means has become a central topic in spintronics. Spin-orbit torques (SOTs)^{1–3} exploit efficient charge-to-spin conversion, typically achieved by the spin Hall effect (SHE) or the spin Rashba-Edelstein effect through the spin-orbit coupling (SOC) of a nonmagnetic metal (NM). The injected spin angular momentum exerts a torque on the magnetization of an adjacent ferromagnetic metal (FM) layer. Recently, an alternative mechanism, known as the orbital torque (OT),^{4–9} has emerged as a new route to control magnetization through orbital angular momentum (OAM) transfer from a NM layer to a FM layer. OTs arise from an OAM current (or simply, orbital current) generated by the orbital Hall effect (OHE), or from an interfacial OAM accumulation by the orbital Rashba-Edelstein effect, both of which can occur even in the absence of SOC.^{10,11} For the transferred OAM to exert a torque on the magnetization of the FM layer, SOC must eventually intervene, since there is no direct exchange coupling between OAM and the local spin moment.⁴ Thus, in contrast to the SOT mechanism, in which the spin current source itself requires SOC to generate spin currents, the OT mechanism assigns the role of SOC in orbital-to-spin conversion to the layer that receives the orbital current, rather than to its source. This mechanism opens a distinct pathway to efficient torque generation using light NMs with weak SOC, drawing increasing attention to the emerging field of orbitronics.^{12–14}

While a variety of light NMs have been examined for OT devices,¹⁴ Ti^{9,15–21} and Cu^{5,6,22–29} are among the most extensively studied materials. Ti is a representative orbital Hall material, as experimentally confirmed through magneto-optical detection¹⁵ and transmission electron microscopy.³⁰ The substantial orbital current generated by the OHE in Ti serves as a source of the OT in Ti/FM bilayers. Although the OHE itself does not require SOC, the OT mechanism relies on orbital-to-spin conversion mediated by SOC. To enhance this conversion efficiency, one typically employs a magnetic layer with stronger SOC²⁰ or inserts a thin heavy metal layer between the Ti and FM layers.^{17,18,21} In this regard, a pronounced dependence on the FM species is a hallmark feature of OT. Notably, even among the *3d* FMs, Ni has been reported to generate larger OTs than other *3d* FMs, which is attributed to its slightly more efficient orbital-to-spin conversion.^{7,8,31–35} This superiority of Ni has also been observed in Ti/FM bilayers.^{9,19} Another remarkable feature of Ti-based OT devices is the long characteristic length in the Ti-thickness dependence, reaching several tens of nanometers.^{9,15,17,19} Although such long-range behavior is not yet fully understood, it indicates that the bulk Ti layer serves as the primary source of the OT.

On the other hand, for Cu-based OT devices, most studies have employed the orbital Rashba-Edelstein effect activated by oxidation of the Cu surface,^{5,6,23–29} rather than the OHE of bulk Cu. In these oxidized Cu/FM structures, enhancement of OT by inserting a heavy metal layer,^{5,25,28} as well as a dependence on the FM species, has been also observed, similar to the behavior in Ti/FM devices. For example, an earlier experiment⁶ reported that the OT is significantly larger when CoFe or Fe is used as the FM, while it becomes negli-

^{a)}Electronic mail: daegeun.jo@physics.uu.se

^{b)}Electronic mail: peter.oppeener@physics.uu.se

gible for Ni and permalloy (Py). This FM dependence appears inconsistent with the SOC-based interpretation established for other OT systems.^{7–9,19,31–35} This seeming discrepancy can be reconciled by attributing the pronounced FM dependence to variations in atomic intermixing at the interface,⁶ whose influence outweighs that of differences in intrinsic SOC. Indeed, large OTs have been reported for both CoFe^{24,26} and Py.^{22,23,27,36} Such diverse FM-dependent behavior raises a key question: to what extent does SOC influence the OT among different 3d FMs?

Addressing this question calls for a comparative theoretical study of OTs in NM/FM bilayers with various combinations of NMs and FMs. Given the long-range behavior of OTs,^{9,15,17,19,33–35,37} it is desirable to investigate sufficiently large bilayer systems, which poses a challenge for fully *ab initio* methods. Although several theoretical studies^{31,37–41} have examined the OT in various heterostructures, a systematic theoretical investigation of the FM dependence of OT in light NM/FM bilayers has, to our knowledge, not yet been performed. It is worth noting that the FM dependence could also originate from a self-induced SOT within the FM layer, also known as the anomalous SOT.⁴² Examining the dependence of the torque on material combination and layer thickness will provide valuable insight into distinguishing OT from other possible contributions.

In this work, we perform a systematic theoretical study of current-induced torques in NM/FM bilayers, where NM = Ti or Cu and FM = Co or Ni. By employing semi-realistic tight-binding models with parameters extracted from *ab initio* calculations, we achieve relatively large system sizes—up to 50 atomic layers ($\gtrsim 10$ nm). For Ti/FM bilayers, we find that the torque is larger for Ni, consistent with experimental observations.^{9,19} For Cu-based systems, we focus on pristine Cu/FM bilayers without oxidation. Although OT in these systems is generally assumed to be negligible, our results reveal non-negligible OT signals, indicating a finite OHE in Cu as predicted theoretically^{43–45} and observed experimentally.^{46,47} Interestingly, the trend of FM dependence reverses in Cu/FM systems under certain conditions, with Co producing a stronger torque. This finding demonstrates that the FM dependence of OT is not universal but can vary depending on the orbital current source, even when only intrinsic effects are considered. We also examine the NM thickness dependence, confirming the bulk NM origin of OTs in both Ti/FM and Cu/FM systems. In Cu/Ni, the bulk Cu contribution exhibits the opposite sign to that in Cu/Co, cautioning that OT cannot be directly predicted from the bulk orbital Hall conductivity of the NM. Consequently, our results demonstrate that the characteristics of OT cannot be explained solely by the individual bulk properties of the NM or FM layers, but depend critically on their material combination. These findings provide microscopic insight into the design of efficient orbitronic devices.

II. THEORETICAL METHODOLOGY

A. Tight-binding models based on *ab initio* electronic structures

We construct semi-realistic tight-binding models for NM/FM systems using the Wannier functions extracted from *ab initio* band structures. The bulk band structures of the NMs (Ti and Cu) and FMs (Co and Ni) are obtained using the full-potential linearized augmented plane-wave code FLEUR.^{48,49} The Perdew-Burke-Ernzerhof functional⁵⁰ within the generalized gradient approximation is used for the exchange-correlation functional. All systems are assumed to have the face-centered cubic (fcc) structure, and the lattice constants of the FMs are set equal to those of the corresponding NMs. Specifically, for Co and Ni, two sets of band structures are independently calculated using either the lattice constant of Ti⁵¹ ($a_{\text{Ti}} = 4.16$ Å) or that of Cu⁵² ($a_{\text{Cu}} = 3.61$ Å), assuming that the FM layer adopts the same structure as the adjoining NM layer in each NM/FM bilayer. The magnetization of Ni and Co is aligned along the normal vector to the fcc(111) plane. SOC is treated within the second variation scheme,⁵³ and the Brillouin zone is sampled using a $12 \times 12 \times 12$ Monkhorst-Pack \mathbf{k} -mesh.⁵⁴

Based on the *ab initio* electronic structures, we use the WANNIER90 code⁵⁵ to construct Wannier functions for each system. Instead of maximally localized Wannier functions, we obtain a set of 18 projected Wannier functions corresponding to the s , p_x , p_y , p_z , d_{xy} , d_{yz} , d_{zx} , d_{z^2} , and $d_{x^2-y^2}$ orbitals for each spin, which yield reasonable accuracy for simple metallic systems.⁵⁶ A uniform $8 \times 8 \times 8$ \mathbf{k} -mesh is used for sampling the Brillouin zone. During the disentanglement procedure, the frozen energy window is defined from the bottom of the valence bands to 5 eV above the Fermi energy. The obtained Wannier function is denoted as $|n\mathbf{R}\rangle$, where n is the band (orbital) index and \mathbf{R} is the lattice vector. The matrix elements of the Hamiltonian \hat{H} and spin $\hat{\mathbf{S}}$ operators, evaluated in the Bloch basis, are transformed into the Wannier representation as $\langle m\mathbf{0}|\hat{H}|n\mathbf{R}\rangle$ and $\langle m\mathbf{0}|\hat{\mathbf{S}}|n\mathbf{R}\rangle$, respectively. The Hamiltonian operator can be decomposed as $\hat{H} = \hat{H}_0 + \hat{H}_{\text{XC}} + \hat{H}_{\text{SOC}}$, where \hat{H}_0 contains the kinetic and potential energies, \hat{H}_{XC} represents the exchange coupling (for Co and Ni), and \hat{H}_{SOC} accounts for SOC. These matrix elements are then used as input parameters for constructing the tight-binding models of the NM/FM bilayers, as described below.

The NM/FM bilayer structures are assumed to be stacked along the (111) direction of the fcc lattice. Each system consists of N_{NM} atomic layers of NM and N_{FM} atomic layers of FM, as illustrated in Fig. 1. The NM/FM bilayer is modeled as a two-dimensional hexagonal lattice with a lattice constant of $a_{\text{NM}}/\sqrt{2}$ and an interlayer spacing of $a_{\text{NM}}/\sqrt{3}$, where a_{NM} ($= a_{\text{Ti}}$ or a_{Cu}) is the bulk lattice constant of the corresponding NM. Based on the bulk Wannier functions $|n\mathbf{R}\rangle$, we con-

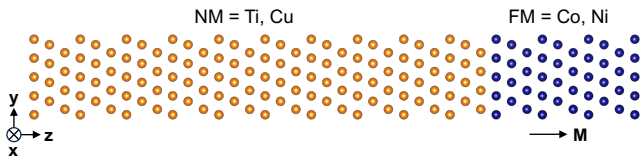


FIG. 1. Illustration of the tight-binding model for the NM/FM bilayer structure with fcc(111) orientation. The presented system is drawn for $N_{\text{NM}} = 30$ and $N_{\text{FM}} = 10$. The system is periodic along x and y directions. The FM layer has an out-of-plane magnetization \mathbf{M} along \hat{z} .

construct the operators $\hat{\mathcal{O}}_{\text{film}}$ for the NM/FM film structure, corresponding to an arbitrary bulk operator $\hat{\mathcal{O}}$, by introducing a set of $18 \times (N_{\text{NM}} + N_{\text{FM}})$ Wannier functions $|n_i \mathbf{R}_{2\text{D}}\rangle$. Here, $\mathbf{R}_{2\text{D}}$ is a two-dimensional lattice vector, and n_i denotes the n orbital in the i -th layer. The Wannier center \mathbf{r}_{n_i} is assumed to coincide with the atomic position \mathbf{r}_i of the i -th layer. The matrix elements $\langle m_j \mathbf{0} | \hat{\mathcal{O}}_{\text{film}} | n_i \mathbf{R}_{2\text{D}} \rangle$, describing hopping between layers i and j , are derived from the corresponding bulk matrix elements $\langle m \mathbf{0} | \hat{\mathcal{O}} | n \mathbf{R} \rangle$ whenever the condition $\mathbf{R}_{2\text{D}} + \mathbf{r}_i - \mathbf{r}_j = \mathbf{R}$ is satisfied. When both layers i and j correspond to the same atomic species, the matrix element in the bilayer is taken to be identical to that of the bulk system. For matrix elements connecting different atomic species, such as hopping terms between NM and FM layers, $\langle m_j \mathbf{0} | \hat{\mathcal{O}}_{\text{film}} | n_i \mathbf{R}_{2\text{D}} \rangle$ is approximated by the average of the bulk values of the two materials. Hereafter, we omit the subscripts in $\langle m_j \mathbf{0} | \hat{\mathcal{O}}_{\text{film}} | n_i \mathbf{R}_{2\text{D}} \rangle$ and simply write $\langle m \mathbf{0} | \hat{\mathcal{O}} | n \mathbf{R} \rangle$ to represent matrix elements for the bilayer system. For the position operator $\hat{\mathbf{r}}$, we define $\langle m \mathbf{0} | \hat{\mathbf{r}} | n \mathbf{R} \rangle = \mathbf{r}_n \delta_{nm} \delta_{0, \mathbf{R}}$, where δ_{nm} is the Kronecker delta.

Once the matrix elements $\langle m \mathbf{0} | \hat{\mathcal{O}} | n \mathbf{R} \rangle$ are obtained ($\hat{\mathcal{O}} = \hat{H}, \hat{\mathbf{S}}, \hat{\mathbf{r}}$), they are interpolated onto a dense 150×150 \mathbf{k} -mesh in momentum space. The Bloch-like states in the Wannier gauge are defined as

$$|\psi_{n\mathbf{k}}^{\text{W}}\rangle = \frac{1}{\sqrt{N}} \sum_{\mathbf{R}} e^{i\mathbf{k}\cdot\mathbf{R}} |n\mathbf{R}\rangle, \quad (1)$$

where N is the number of lattice vectors. The corresponding operator matrix elements in the Wannier gauge are then given by

$$\mathcal{O}_{mn}^{\text{W}}(\mathbf{k}) = \langle \psi_{m\mathbf{k}}^{\text{W}} | \hat{\mathcal{O}} | \psi_{n\mathbf{k}}^{\text{W}} \rangle = \frac{1}{N} \sum_{\mathbf{R}} e^{i\mathbf{k}\cdot\mathbf{R}} \langle m \mathbf{0} | \hat{\mathcal{O}} | n \mathbf{R} \rangle. \quad (2)$$

Since $|\psi_{n\mathbf{k}}^{\text{W}}\rangle$ is not an eigenstate of the Hamiltonian, the eigenstates $|\psi_{n\mathbf{k}}\rangle$ and eigenvalues $\epsilon_{n\mathbf{k}}$, satisfying $\hat{H}|\psi_{n\mathbf{k}}\rangle = \epsilon_{n\mathbf{k}}|\psi_{n\mathbf{k}}\rangle$, are obtained by diagonalizing $\hat{H}^{\text{W}}(\mathbf{k})$. The resulting matrix elements $\langle \psi_{m\mathbf{k}} | \hat{\mathcal{O}} | \psi_{n\mathbf{k}} \rangle$ in the Hamiltonian gauge are then used in the linear-response calculation, as described in the following subsection.

B. Linear-response calculation of the current-induced torque

The current-induced torques in NM/FM bilayers are calculated within the framework of linear-response theory. Under an in-plane electric field $\mathbf{E} = E_x \hat{x}$, the induced torque generally contains two components: a field-like torque $\propto \hat{\mathbf{M}} \times \hat{y}$ and a damping-like torque $\propto \hat{\mathbf{M}} \times (\hat{\mathbf{M}} \times \hat{y})$, where $\hat{\mathbf{M}}$ is the unit vector of magnetization.¹ For an out-of-plane magnetization in the FM, i.e., $\hat{\mathbf{M}} = \hat{z}$, the field-like and damping-like torques are directed along \hat{x} and \hat{y} , respectively. In this work, we focus on the damping-like torque, which has been primarily investigated in orbitronics¹⁴ and is known to play a crucial role in SOT device functionalities.³

Within linear-response theory, the torque \mathbf{T} induced by the electric field \mathbf{E} is expressed as

$$T_i = t_{ij} E_j, \quad (3)$$

where t_{ij} is the component of the linear-response tensor \mathbf{t} , referred to as the torkance, and i and j denote Cartesian components. In the Kubo formalism, t_{ij} is decomposed into intraband and interband contributions, $t_{ij} = t_{ij}^{\text{intra}} + t_{ij}^{\text{inter}}$, each of which is evaluated as follows:^{31,57}

$$t_{ij}^{\text{intra}} = \frac{e\hbar}{\Gamma} \int \frac{d^2\mathbf{k}}{(2\pi)^2} \sum_n \left(\frac{\partial f_{n\mathbf{k}}}{\partial \epsilon_{n\mathbf{k}}} \right) \times \langle \psi_{n\mathbf{k}} | \hat{T}_i | \psi_{n\mathbf{k}} \rangle \langle \psi_{n\mathbf{k}} | \hat{v}_j | \psi_{n\mathbf{k}} \rangle, \quad (4)$$

$$t_{ij}^{\text{inter}} = -e\hbar \int \frac{d^2\mathbf{k}}{(2\pi)^2} \sum_{n \neq m} (f_{n\mathbf{k}} - f_{m\mathbf{k}}) \times \text{Im} \left[\frac{\langle \psi_{n\mathbf{k}} | \hat{T}_i | \psi_{m\mathbf{k}} \rangle \langle \psi_{m\mathbf{k}} | \hat{v}_j | \psi_{n\mathbf{k}} \rangle}{(\epsilon_{n\mathbf{k}} - \epsilon_{m\mathbf{k}})(\epsilon_{n\mathbf{k}} - \epsilon_{m\mathbf{k}} + i\Gamma)} \right], \quad (5)$$

where $e > 0$ is the elementary charge, $f_{n\mathbf{k}} = 1/[e^{(\epsilon_{n\mathbf{k}} - \mu)/k_B T} + 1]$ is the Fermi-Dirac distribution function, with the chemical potential μ and $k_B T = 25$ meV, $\hat{\mathbf{v}} = \frac{i}{\hbar} [\hat{H}, \hat{\mathbf{r}}]$ is the velocity operator, and $\hat{\mathbf{T}} = \frac{i}{\hbar} [\hat{H}_{\text{XC}}, \hat{\mathbf{S}}]$ is the exchange torque operator. The effect of disorder is approximately described by a constant energy broadening Γ . The OAM current or accumulation is not explicitly considered in the torque calculations using Eqs. (4) and (5), but its contribution to the OT is implicitly included.³¹ The intraband term t_{ij}^{intra} in Eq. (4) corresponds to the (Drude-like) Boltzmann contribution, which scales with the momentum relaxation time $\tau \propto 1/\Gamma$. In contrast, the interband term t_{ij}^{inter} in Eq. (5) arises from the Berry curvature mechanism and represents an intrinsic contribution. Notably, t_{ij}^{intra} and t_{ij}^{inter} are odd and even under time-reversal, respectively. Symmetry considerations indicate that t_{ij}^{intra} gives rise to the field-like torque, whereas t_{ij}^{inter} leads to the damping-like torque.³¹ Therefore, we calculate only $t_{yx}^{\text{inter}} \equiv t_{yx}$ to describe the damping-like torque induced by an electric field applied along \hat{x} .

III. RESULTS AND DISCUSSION

A. Phenomenological mechanism

Before presenting the numerical results, we first discuss the phenomenology of the current-induced torques in NM/FM bilayers. It is important to note that our calculations yield the total current-induced torque acting on the magnetization, rather than the OT contribution alone. While the damping-like torque evaluated by Eq. (5) originates from intrinsic mechanisms, multiple contributions may coexist, including OT, SOT, and self-induced torque within the FM layer.³¹ For Ti/FM and Cu/FM bilayers, however, the SOT contribution can be safely neglected since both Ti and Cu exhibit negligible SHEs.^{43–45} Therefore, our calculations mainly capture the OT or self-induced torque components. Distinguishing these contributions unambiguously is generally nontrivial, both theoretically and experimentally. Below, we discuss the physical mechanisms underlying these two torques and their expected dependences on the FM species and NM thickness.

Let us consider a light NM/FM bilayer structure, where the SOC in the NM is negligible, such that it creates only orbital currents but not spin currents. The FM is assumed to possess weak SOC that nevertheless allows moderate orbital-to-spin conversion. We confine our discussion to intrinsic effects governed by the electronic band structure and disregard extrinsic factors such as crystallinity or interfacial quality. Figure 2(a) illustrates how an orbital current generated in the NM gives rise to an OT on the FM layer.⁴ When the orbital current transmits across the NM/FM interface, it undergoes intrinsic relaxation and is absorbed into the lattice and spin degrees of freedom via the crystal field and SOC, respectively. Even if a significant portion of the OAM is quenched by the crystal field, the remaining OAM can still lead to a substantial torque on the FM layer. The torque efficiency is then determined by how effectively the OAM couples to the local spin moment through SOC and exchange interaction, competing with quenching due to the crystal field. Therefore, the OT mechanism inherently depends on the FM's intrinsic properties, particularly its SOC, which governs the efficiency of orbital-to-spin conversion. Additional factors such as interface transparency⁵⁸ or orbital texture matching between the NM and FM layers¹⁹ may also play a role, though their effects are not yet fully understood.

Meanwhile, the orbital current may originate either from the bulk or from a confined interfacial region. If it is generated only near the interface, its contribution to the OT should be largely independent of NM thickness. In contrast, if the orbital current is generated in the NM bulk, the transferred OAM, and thus the OT, should increase with increasing NM thickness, up to a characteristic length scale associated with OAM generation in the NM layer. This length scale is not necessarily identical to the orbital diffusion length. Considering that both the

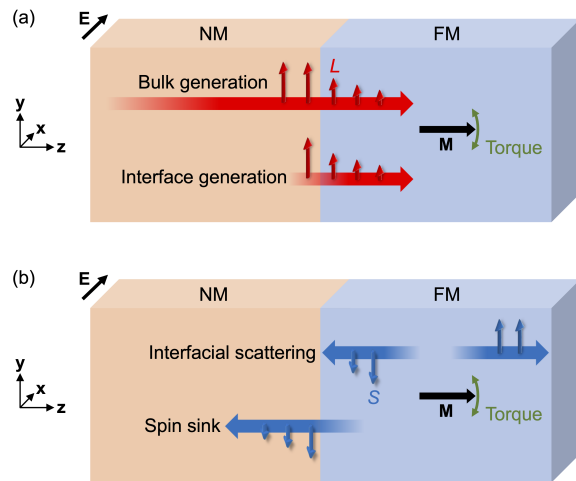


FIG. 2. Schematic illustration of the (a) OT and (b) self-induced SOT in a NM/FM bilayer. The red and blue arrows represent the OAM (L) and spin (S), respectively. For each case, two possible contributions associated with the bulk NM and the NM/FM interface are shown.

intrinsic OHE¹⁰ and the damping-like torque described by Eq. (5) arise from interband coherence in response to the electric field, the thickness dependence may also reflect an interband coherence length. The relevant characteristic length may therefore vary with the regime of OAM transport, which remains under active debate.^{59–63}

We now turn to the self-induced SOT, illustrated in Fig. 2(b). We consider a situation in which the bulk FM generates a spin current via the SHE, leading to spin accumulation within the FM layer itself. In an inversion symmetric geometry—e.g., a FM layer sandwiched between identical top and bottom contacts—the spin accumulations at the two interfaces have the same magnitude with opposite signs, so the resulting torque cancels out. In a NM/FM bilayer, however, the lack of inversion symmetry causes the spin accumulation at the NM/FM interface and at the opposite FM surface to differ, producing a net SOT. Because the spin Hall conductivity varies substantially across $3d$ FMs,^{44,45,64} this self-induced SOT also strongly depends on the choice of FM.⁴² A recent experiment⁶⁵ reported that the FM dependence of the current-induced torque in Ta/FM bilayers originates predominantly from such a self-induced SOT, rather than the OT. It should be noted, however, that the self-induced SOT, despite its self-generating origin, depends critically not only on the material combination but also on the NM thickness, as discussed below.

The imbalance in spin accumulation can be induced by two different mechanisms. The first is an interfacial contribution, where inequivalent interfaces lead to different local spin accumulations at the top and bottom surfaces of the FM, irrespective of the bulk NM region. Such asymmetry can result from variations in interfacial spin scattering at the NM/FM interface,⁶⁶ which are typically

material-specific. The resulting torque is expected to be largely independent of the NM thickness. The second is a bulk contribution, where the NM acts as a spin sink. When the spin current generated within the FM layer is injected into the NM layer, it experiences relaxation via the SOC of the NM bulk. The greater the spin absorption by the NM, the larger the resulting torque. Consequently, this contribution increases with NM thickness, where the relevant characteristic length is determined by the spin relaxation length of the NM. However, the spin relaxation length is typically significantly long in light NMs due to weak SOC, which implies that they are inefficient spin sinks.⁶⁷ If the NM layer is thinner than its spin diffusion length, the spin current will be only weakly absorbed. Therefore, in nanoscale NM/FM bilayers, the self-induced SOT is expected to be much weaker for light NMs than for heavy NMs such as Ta.⁶⁵

Finally, we note that, in addition to the SHE, a considerable OHE can also occur in $3d$ FMs.^{44,45} This suggests the possibility of a self-induced OT arising through a similar mechanism, which, to the best of our knowledge, has not been reported before. In that case, the NM-thickness dependence of the torque would be governed by the orbital relaxation length, instead of the spin relaxation length. Importantly, this length scale is likely different from that of the OT, since the orbital sink mechanism would involve diffusive OAM relaxation rather than its coherent generation. Similarly, a distinction between the characteristic length scales for Ti measured in OT experiments (where the orbital current is injected from the NM to the FM) and in orbital pumping experiments (where the orbital current flows in the opposite direction) was recently discussed.⁶⁸

B. Current-induced torques in Ti/FM and Cu/FM

Figure 3(a) presents the damping-like component of the torkance $t_{yx} = t_{yx}^{\text{inter}}$ evaluated from Eq. (5) for Ti/FM and Cu/FM bilayers, where FM is either Co or Ni. The layer numbers are set to $N_{\text{NM}} = 20$ and $N_{\text{FM}} = 10$. All systems exhibit a negative t_{yx} , corresponding to the sign of the current-induced torque expected for NMs with positive spin or orbital Hall conductivity.^{31,57} The sign of t_{yx} is thus consistent with the positive orbital Hall conductivities of Ti and Cu reported in earlier theoretical works,^{43,44} although a more recent study predicted a negative orbital Hall conductivity for Cu.⁴⁵ However, caution is warranted, as the theoretical evaluation of orbital Hall conductivity is not yet fully established. The conventional definition of orbital Hall conductivity^{10,43,44,69,70} is based on the conventional orbital current operator $\hat{J}_i^{L_j} = \frac{1}{2}(\hat{v}_i \hat{L}_j + \hat{L}_j \hat{v}_i)$. This definition often provides qualitatively reasonable agreement with experiments,^{71,72} but its calculated value varies considerably across different theoretical approaches.^{44,45,73,74} Moreover, the definition of $\hat{J}_i^{L_j}$ itself possesses an inherent limitation stemming from the non-

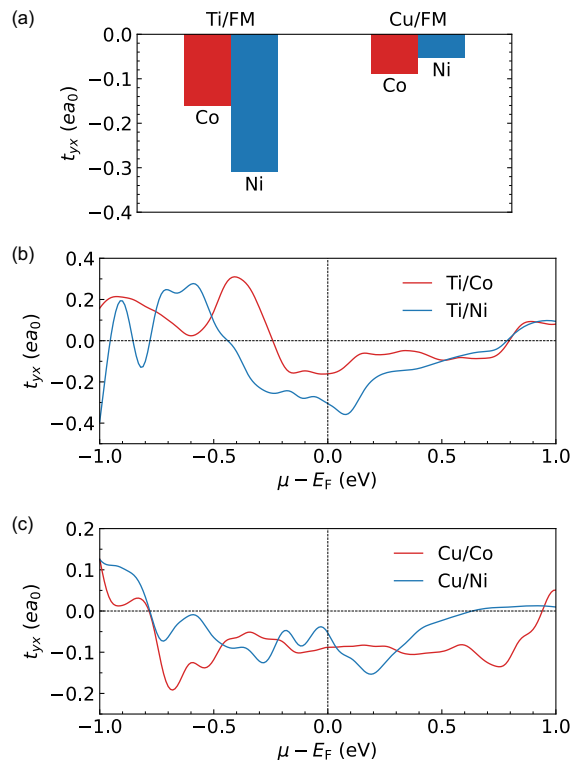


FIG. 3. (a) Torkance t_{yx} in Ti/FM and Cu/FM bilayers (FM = Co, Ni) with $N_{\text{NM}} = 20$ and $N_{\text{FM}} = 10$. Chemical potential dependence of t_{yx} in (b) Ti/FM and (c) Cu/FM bilayers.

conservation of OAM in crystals.^{15,75,76} The orbital current undergoes a significant change due to sources such as the crystal field. Establishing a link between the conventional orbital current and experimentally measurable quantities thus requires accounting for the non-conserved part of OAM. Our approach circumvents these issues by directly computing the well-defined observable, the torque exerted on the magnetization, without explicitly invoking OAM.

For Ti/FM bilayers, we obtain $t_{yx} = -0.16 ea_0$ for Ti/Co and $t_{yx} = -0.31 ea_0$ for Ti/Ni. Both values are notably large, comparable to those calculated for conventional SOT systems employing heavy NMs such as Pt and W.^{31,57} When Ti is replaced by Cu, the torque magnitude is reduced but remains finite: $t_{yx} = -0.088 ea_0$ for Cu/Co and $t_{yx} = -0.053 ea_0$ for Cu/Ni. This indicates that, even without oxidation, Cu can intrinsically generate a measurable torque. The result aligns with theoretical predictions that Cu hosts a finite OHE despite its predominantly s -orbital character,^{43–45} and with experimental reports of OHE in Cu,^{46,47} though a quantitative comparison remains difficult.

A key finding of this work is that the FM dependence of the OT in NM/FM bilayers varies depending on the NM species. For Ti/FM, Ni yields a larger torque than Co, which is consistent with experimentally observed large torques in Ti/Ni devices^{9,15,19} and with the established

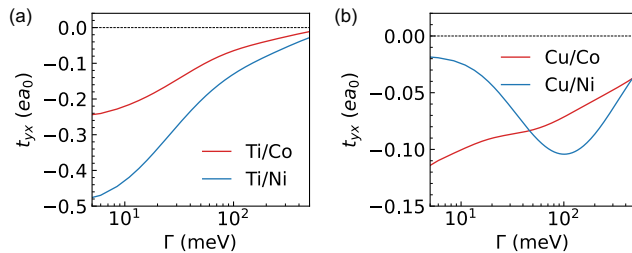


FIG. 4. (a) Torkance t_{yx} as a function of the broadening energy Γ in (a) Ti/FM and (b) Cu/FM bilayers (FM = Co, Ni) with $N_{\text{NM}} = 20$ and $N_{\text{FM}} = 10$.

understanding that Ni's stronger SOC enables more efficient orbital-to-spin conversion. This trend persists across a broad chemical potential range near the Fermi level, as shown in Fig. 3(b). Within the OT mechanism, the sign reversal of t_{yx} with decreasing energy reflects the energy-dependent spin-orbit correlation of the FM.^{4,7} The peak near -0.35 eV for Ti/Co is slightly shifted from the peak near -0.6 eV for Ti/Ni because Ni has one additional d electron. Hence, the results for Ti can be reasonably explained in terms of the FM's spin-orbit correlation.

In contrast, for Cu/FM bilayers, the torque is larger for Co than Ni. Moreover, the energy dependence of t_{yx} in Fig. 3(c) does not show a clear trend between Cu/Co and Cu/Ni. This suggests that the orbital-to-spin efficiency is not the dominant factor governing the FM dependence in these systems; instead, other factors—such as interface transparency⁵⁸ or orbital texture matching¹⁹—may play more decisive roles. This interpretation is reasonable considering that Ni and Co are adjacent in the Periodic Table and thus their SOC strengths are not dramatically different. Furthermore, we note that the observed behavior cannot be attributed to self-induced SOT, since Ni exhibits a substantially larger spin Hall conductivity than Co.^{44,45}

The disorder effect is modeled by introducing a constant broadening Γ in Eq. (5). Figure 4(a) shows that in Ti/FM systems, t_{yx} decreases monotonically as Γ increases, while the relative FM dependence remains robust. The enhancement of torque when using Ni instead of Co is roughly twofold at most, consistent with its slightly stronger SOC of Ni. Figure 4(b) displays the Γ dependence for Cu/FM systems. Interestingly, Cu/Ni exhibits a non-monotonic dependence, attributable to the sharp energy dependence of t_{yx} near the Fermi level [see Fig. 3(c)]. As a result, Co yields a larger torque in the clean limit, whereas Ni produces a larger torque in the intermediate disorder regime. These results demonstrate that even for a fixed NM, the FM dependence of OT can vary, highlighting that there is no universal rule for selecting an optimal FM. Instead, the dependence varies strongly with the specific NM-FM combination and intrinsic factors such as disorder.

C. Dependence on NM thickness: bulk origin of OT

As discussed in Sec. III A, the calculated torkance t_{yx} includes not only the OT originating from the bulk orbital current in NMs but also possible contributions from the FM and the NM/FM interface. To identify the bulk NM origin in our systems, we examine the dependence of t_{yx} on the NM layer thickness.

Figures 5(a)-5(d) show t_{yx} as a function of the broadening energy Γ for various NM layer numbers N_{NM} , while $N_{\text{FM}} = 10$ is fixed. For $N_{\text{NM}} = 1$, the NM bulk contribution is expected to be negligible, so the torque mainly originates from the NM/FM interface. As N_{NM} increases, the bulk contribution becomes more pronounced, while the interfacial contribution would remain nearly unchanged. Comparing the results for $N_{\text{Ti}} = 1$ and $N_{\text{Ti}} = 40$ [Figs. 5(a) and 5(b)], we find that the bulk Ti contribution dominates once the Ti layer becomes sufficiently thick for both Ti/Co and Ti/Ni. In particular, the thickness dependence becomes more prominent as Γ decreases, while it weakens for $\Gamma \gtrsim 100$ meV.

Noticeable thickness dependences of t_{yx} are also observed in Cu/FM bilayers [Figs. 5(c) and 5(d)]. Interestingly, for Cu/Ni, the variation of t_{yx} with N_{Cu} reverses sign between clean and disordered regimes. For $\Gamma \lesssim 30$ meV, t_{yx} increases in the positive direction with N_{Cu} , implying that the Cu bulk contribution in this regime has the opposite sign to the OT expected for a positive orbital Hall conductivity. Consequently, the total torque becomes positive in the thick limit, unlike in other systems. This sign reversal recalls the ambiguity in the theoretically predicted sign of the orbital Hall conductivity of Cu. In addition, as discussed in Sec. III B, the conventional definition of the orbital Hall conductivity does not account for the non-conservation of OAM in crystals, an effect that is implicitly taken into account in the torque calculation.³¹ In this regard, our results reveal a possible discrepancy between the theoretically calculated bulk orbital Hall conductivity and the effective orbital Hall conductivity measured in OT experiments.

To more clearly visualize the thickness dependence, we plot t_{yx} as a function of N_{NM} for two selected broadening energies, $\Gamma = 10$ meV and $\Gamma = 100$ meV, corresponding to the clean and disordered regimes, respectively [Figs. 5(e)-5(h)]. The torque is strongly suppressed for $N_{\text{NM}} = 1$, indicating a minor interfacial contribution in all cases. This aligns with experiments that report negligible damping-like torque in NM/Py devices with ultrathin (~ 0.5 nm) Ti and Cu layers.⁷⁷ For Ti/FM [Fig. 5(f)], the torque saturates rapidly, which seems to agree with recent first-principles results showing a fast decay of orbital currents within a few atomic layers.⁵⁹ However, we note that Ref.⁵⁹ investigated orbital currents injected from the FM, which differs from the OT mechanism considered here. Indeed, Fig. 5(e) shows that the torque does not fully saturate even for $N_{\text{Ti}} = 40$ (≈ 9.6 nm). Such a long characteristic length—well beyond atomic scales—shows qualitative agreement with

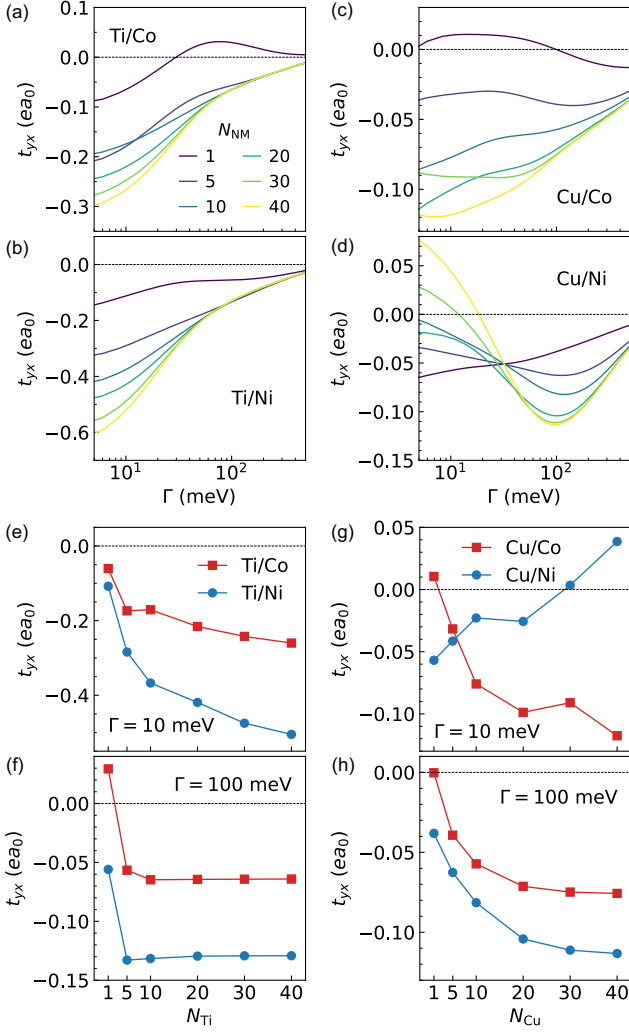


FIG. 5. Torkance t_{yx} as a function of the broadening energy Γ in (a) Ti/Co, (b) Ti/Ni, (c) Cu/Co, and (d) Cu/Ni bilayers, with $N_{NM} = 1, 5, 10, 20, 30, 40$ and $N_{FM} = 10$. (e),(f) N_{Ti} dependence of t_{yx} in Ti/FM bilayers for $\Gamma = 10$ meV and $\Gamma = 100$ meV. (g),(h) N_{Cu} dependence of t_{yx} in Cu/FM bilayers for $\Gamma = 10$ meV and $\Gamma = 100$ meV.

experimental observations of long-range OT in Ti/FM devices.^{9,15,17,19,20}

A similarly long-range behavior is found in Cu/FM systems. As noted above, the opposite Cu bulk contribution in Cu/Ni in the clean regime is clearly visible in Fig. 5(g). Interestingly, the characteristic length in Cu/FM systems remains relatively robust even for $\Gamma = 100$ meV [Fig. 5(h)], unlike Ti/FM, where the length shortens considerably with increasing disorder. The distinct thickness dependences between Ti/FM and Cu/FM thus warrant further investigation. Also, a more quantitative analysis would require explicit treatment of extrinsic scattering, which is beyond the scope of this work.

Finally, we emphasize that the NM bulk contribution mainly originates from the OT. Although both OT and self-induced SOT can, in principle, depend on NM thick-

ness (see Sec. III A), the latter contribution is likely minor for two reasons. First, first-principles calculations show that the spin Hall conductivity of ferromagnetic Ni is significantly large, comparable to that of Pt, whereas that of ferromagnetic Co is negligible.⁴⁵ In our calculations, however, the torques in NM/Co and NM/Ni are of the same order of magnitude. Second, the length scale of a self-induced SOT is governed by the spin diffusion length of the NM, which can reach several hundred nanometers in light NMs such as Cu.⁷⁸ By contrast, the thickness dependence observed here extends only up to about 10 nm, suggesting a much shorter relevant length scale. Meanwhile, we note that the possibility of a self-induced OT cannot be entirely ruled out. The orbital Hall conductivities for Co and Ni are comparable,^{44,45} and an orbital diffusion length on the order of a few nanometers is plausible. A clear identification and separation of such effects are left for future work.

IV. CONCLUSION

In this work, we examined current-induced torques in NM/FM bilayers using semi-realistic tight-binding models constructed from first-principles electronic structures. By directly evaluating the torque in heterostructures, our approach provides quantitative results without relying on a simplified picture based on the bulk properties of individual NM and FM layers. We systematically investigated the torque depending on material combination and NM layer thickness. Our results show that both Ti/FM and Cu/FM bilayers exhibit sizable damping-like torques, ascribed to the OAM generation in the bulk NMs. The dependence on the FM choice between Co and Ni, however, differs between Ti and Cu systems: Ni yields a larger torque in Ti/FM, whereas Co produces a stronger torque in Cu/FM. This contrasting behavior indicates that the FM-dependent OT efficiency is not governed solely by the SOC strength of the FM but is also strongly affected by orbital hybridization or interfacial characteristics across the NM/FM interface. Thickness-dependent analyses further reveal that the torque predominantly arises from the NM bulk, confirming the bulk nature of the OT. The sign of the OT does not necessarily coincide with that of the bulk orbital Hall conductivity, as also indicated by a recent experiment,⁷⁹ calling for careful assessment of sign determination in OT measurements. The characteristic length ranges from the atomic scale to over 10 nm, depending on the disorder strength. These findings provide valuable guidance for engineering efficient OT devices based on light metals.

ACKNOWLEDGMENTS

This work was supported by the Swedish Research Council (VR), the Knut and Alice Wallenberg Foundation (Grants No. 2022.0079 and No. 2023.0336), and the

Wallenberg Initiative Materials Science for Sustainability (WISE) funded by the Knut and Alice Wallenberg Foundation. We further acknowledge support from the EIC Pathfinder OPEN grant No. 101129641 “OBELIX”. The calculations were supported by resources provided by the National Academic Infrastructure for Supercomputing in Sweden (NAISS) at NSC Linköping, partially funded by VR through Grant No. 2022-06725.

- ¹A. Manchon, J. Železný, I. M. Miron, T. Jungwirth, J. Sinova, A. Thiaville, K. Garello, and P. Gambardella, “Current-induced spin-orbit torques in ferromagnetic and antiferromagnetic systems,” *Rev. Mod. Phys.* **91**, 035004 (2019).
- ²X. Han, X. Wang, C. Wan, G. Yu, and X. Lv, “Spin-orbit torques: Materials, physics, and devices,” *Applied Physics Letters* **118**, 120502 (2021).
- ³Q. Shao, P. Li, L. Liu, H. Yang, S. Fukami, A. Razavi, H. Wu, K. Wang, F. Freimuth, Y. Mokrousov, M. D. Stiles, S. Emori, A. Hoffmann, J. Åkerman, K. Roy, J.-P. Wang, S.-H. Yang, K. Garello, and W. Zhang, “Roadmap of spin-orbit torques,” *IEEE Transactions on Magnetics* **57**, 1–39 (2021).
- ⁴D. Go and H.-W. Lee, “Orbital torque: Torque generation by orbital current injection,” *Phys. Rev. Res.* **2**, 013177 (2020).
- ⁵S. Ding, A. Ross, D. Go, L. Baldrati, Z. Ren, F. Freimuth, S. Becker, F. Kammerbauer, J. Yang, G. Jakob, Y. Mokrousov, and M. Kläui, “Harnessing Orbital-to-Spin Conversion of Interfacial Orbital Currents for Efficient Spin-Orbit Torques,” *Phys. Rev. Lett.* **125**, 177201 (2020).
- ⁶J. Kim, D. Go, H. Tsai, D. Jo, K. Kondou, H.-W. Lee, and Y. Otani, “Nontrivial torque generation by orbital angular momentum injection in ferromagnetic-metal/Cu/Al₂O₃ trilayers,” *Phys. Rev. B* **103**, L020407 (2021).
- ⁷D. Lee, D. Go, H.-J. Park, W. Jeong, H.-W. Ko, D. Yun, D. Jo, S. Lee, G. Go, J. H. Oh, K.-J. Kim, B.-G. Park, B.-C. Min, H. C. Koo, H.-W. Lee, O. Lee, and K.-J. Lee, “Orbital torque in magnetic bilayers,” *Nature Communications* **12**, 6710 (2021).
- ⁸S. Lee, M.-G. Kang, D. Go, D. Kim, J.-H. Kang, T. Lee, G.-H. Lee, J. Kang, N. J. Lee, Y. Mokrousov, S. Kim, K.-J. Kim, K.-J. Lee, and B.-G. Park, “Efficient conversion of orbital Hall current to spin current for spin-orbit torque switching,” *Communications Physics* **4**, 234 (2021).
- ⁹H. Hayashi, D. Jo, D. Go, T. Gao, S. Haku, Y. Mokrousov, H.-W. Lee, and K. Ando, “Observation of long-range orbital transport and giant orbital torque,” *Communications Physics* **6**, 32 (2023).
- ¹⁰D. Go, D. Jo, C. Kim, and H.-W. Lee, “Intrinsic Spin and Orbital Hall Effects from Orbital Texture,” *Phys. Rev. Lett.* **121**, 086602 (2018).
- ¹¹L. Salemi, M. Berritta, A. K. Nandy, and P. M. Oppeneer, “Orbitally dominated Rashba-Edelstein effect in noncentrosymmetric antiferromagnets,” *Nature Communications* **10**, 5381 (2019).
- ¹²D. Go, D. Jo, H.-W. Lee, M. Kläui, and Y. Mokrousov, “Orbitronics: Orbital currents in solids,” *Europhysics Letters* **135**, 37001 (2021).
- ¹³D. Jo, D. Go, G.-M. Choi, and H.-W. Lee, “Spintronics meets orbitronics: Emergence of orbital angular momentum in solids,” *npj Spintronics* **2**, 1–9 (2024).
- ¹⁴K. Ando, “Orbitronics: Harnessing Orbital Currents in Solid-State Devices,” *Journal of the Physical Society of Japan* **94**, 092001 (2025).
- ¹⁵Y.-G. Choi, D. Jo, K.-H. Ko, D. Go, K.-H. Kim, H. G. Park, C. Kim, B.-C. Min, G.-M. Choi, and H.-W. Lee, “Observation of the orbital Hall effect in a light metal Ti,” *Nature* **619**, 52–56 (2023).
- ¹⁶Q. Zhao, X. Luo, H. Wu, B. He, Q. Wang, T. Zhang, Z. Li, P. Liu, C. Zhao, J. Wang, Q. Liu, G. Yu, and J. Wei, “Efficient Charge-to-Orbit Current Conversion for Orbital Torque Based Artificial Neurons and Synapses,” *Advanced Electronic Materials* **11**, 2400721 (2025).
- ¹⁷X. Xu, D. Zhang, Y. Wang, L. Zhang, Y. Qu, Z. Zhong, F. Bai, X. Tang, Q. Yang, H. Zhang, and L. Jin, “Observation of Giant Effective Orbital Hall Angle in Ti/Pt Metallic Heterostructure,” *Small* **21**, 2408721 (2025).
- ¹⁸S. y. Shin, D. Han, S. Lee, and B.-G. Park, “Enhanced Magnetization Switching Efficiency via Orbital-Current-Induced Torque in Ti/Ta (Pt)/CoFeB/MgO Structures,” *Advanced Functional Materials* **35**, 2425932 (2025).
- ¹⁹H. Hayashi, J. Chen, D. Jo, S. Sakamoto, T. Gao, D. Go, Y. Mokrousov, H.-W. Lee, S. Miwa, and K. Ando, “Crystallographic Engineering for Enhanced Orbital Torque,” *Nano Letters* **25**, 15124–15129 (2025).
- ²⁰T. Xu, A. Tang, K. Wang, W. Wei, Y. Liu, and H. Du, “Orbital torque switching of perpendicular magnetization in Ti/ferrimagnet bilayers,” *The Innovation Materials* , 100158 (2025).
- ²¹D. Zheng, J. Xu, F. Alsayafi, S. Krishnia, D. Go, D. Tran, T. Yang, Y. Li, Y. Ma, C. Liu, M. Tang, A. Chen, H. Algaidi, H. Wu, K. Liu, Y. Mokrousov, M. Kläui, U. Schwingenschlögl, and X. Zhang, “Manipulating magnetization by orbital current from a light metal Ti,” (2025), arXiv:2504.04399 [cond-mat.mtrl-sci].
- ²²H. An, Y. Kageyama, Y. Kanno, N. Enishi, and K. Ando, “Spin-torque generator engineered by natural oxidation of Cu,” *Nature Communications* **7**, 13069 (2016).
- ²³Y. Tazaki, Y. Kageyama, H. Hayashi, T. Harumoto, T. Gao, J. Shi, and K. Ando, “Current-induced torque originating from orbital current,” (2020), arXiv:2004.09165 [cond-mat.mtrl-sci].
- ²⁴J. Kim, J. Uzuhashi, M. Horio, T. Senoo, D. Go, D. Jo, T. Sumi, T. Wada, I. Matsuda, T. Ohkubo, S. Mitani, H.-W. Lee, and Y. Otani, “Oxide layer dependent orbital torque efficiency in ferromagnet/Cu/oxide heterostructures,” *Phys. Rev. Mater.* **7**, L111401 (2023).
- ²⁵S. Krishnia, B. Bony, E. Rongione, L. M. Vicente-Arche, T. Denneulin, A. Pezo, Y. Lu, R. E. Dunin-Borkowski, S. Collin, A. Fert, J.-M. George, N. Reyren, V. Cros, and H. Jaffrès, “Quantifying the large contribution from orbital Rashba–Edelstein effect to the effective damping-like torque on magnetization,” *APL Materials* **12**, 051105 (2024).
- ²⁶S. Ding, H. Wang, W. Legrand, P. Noël, and P. Gambardella, “Mitigation of Gilbert Damping in the CoFe/CuOx Orbital Torque System,” *Nano Letters* **24**, 10251–10257 (2024).
- ²⁷S. Damerio and C. O. Avci, “Tunable Spin and Orbital Torques in Cu-Based Magnetic Heterostructures,” *Nano Letters* **25**, 2181–2187 (2025).
- ²⁸C.-J. Li and C.-F. Pai, “Oxidation-Tuned CuOx for Spin–Orbit Torque Efficiency Enhancement,” *ACS Applied Materials & Interfaces* (2025), 10.1021/acsaami.5c15854.
- ²⁹L. Yi, T. Yang, C. Tan, R. Xie, S. Liu, L. Cai, Q. Cao, Y. Wang, W. Lü, Y. Tian, Q. Huang, and S. Yan, “Large Orbital Torque from Interfacial Spin-Vorticity Coupling in PtCo/Cu Heterostructures,” *Phys. Rev. Lett.* **135**, 156702 (2025).
- ³⁰J. C. Idrobo, J. Ruzs, G. Datt, D. Jo, S. Alikhah, D. Muradas, U. Nounbe, M. V. Kamalakar, and P. M. Oppeneer, “Direct observation of nanometer-scale orbital angular momentum accumulation,” (2024), arXiv:2403.09269 [cond-mat.mes-hall].
- ³¹D. Go, F. Freimuth, J.-P. Hanke, F. Xue, O. Gomonay, K.-J. Lee, S. Blügel, P. M. Haney, H.-W. Lee, and Y. Mokrousov, “Theory of current-induced angular momentum transfer dynamics in spin-orbit coupled systems,” *Phys. Rev. Res.* **2**, 033401 (2020).
- ³²S. Dutta and A. A. Tulapurkar, “Observation of nonlocal orbital transport and sign reversal of dampinglike torque in Nb/Ni and Ta/Ni bilayers,” *Phys. Rev. B* **106**, 184406 (2022).
- ³³A. Bose, F. Kammerbauer, R. Gupta, D. Go, Y. Mokrousov, G. Jakob, and M. Kläui, “Detection of long-range orbital-Hall torques,” *Phys. Rev. B* **107**, 134423 (2023).
- ³⁴R. Fukunaga, S. Haku, H. Hayashi, and K. Ando, “Orbital torque originating from orbital Hall effect in Zr,” *Phys. Rev. Res.* **5**, 023054 (2023).

- ³⁵H. Moriya, M. Taniguchi, D. Jo, D. Go, N. Soya, H. Hayashi, Y. Mokrousov, H.-W. Lee, and K. Ando, "Observation of Long-Range Current-Induced Torque in Ni/Pt Bilayers," *Nano Letters* **24**, 6459–6464 (2024).
- ³⁶G. Okano, M. Matsuo, Y. Ohnuma, S. Maekawa, and Y. Nozaki, "Nonreciprocal Spin Current Generation in Surface-Oxidized Copper Films," *Phys. Rev. Lett.* **122**, 217701 (2019).
- ³⁷D. Go, D. Jo, K.-W. Kim, S. Lee, M.-G. Kang, B.-G. Park, S. Blügel, H.-W. Lee, and Y. Mokrousov, "Long-Range Orbital Torque by Momentum-Space Hotspots," *Phys. Rev. Lett.* **130**, 246701 (2023).
- ³⁸L. Salemi, M. Berritta, and P. M. Oppeneer, "Quantitative comparison of electrically induced spin and orbital polarizations in heavy-metal/*3d*-metal bilayers," *Phys. Rev. Mater.* **5**, 074407 (2021).
- ³⁹S. A. Nikolaev, M. Chshiev, F. Ibrahim, S. Krishnia, N. Sebe, J.-M. George, V. Cros, H. Jaffrès, and A. Fert, "Large Chiral Orbital Texture and Orbital Edelstein Effect in Co/Al Heterostructure," *Nano Letters* **24**, 13465–13472 (2024).
- ⁴⁰H. Devda, A. Deák, L. Salemi, L. Rózsa, L. Szunyogh, P. M. Oppeneer, and U. Nowak, "Anatomy of spin-orbit-torque-assisted magnetization dynamics in Co/Pt bilayers: Importance of the orbital torque," *Phys. Rev. B* **112**, 144438 (2025).
- ⁴¹A. Pezo, N. Sebe, A. Manchon, V. Cros, and H. Jaffrès, "Anatomy of torques from orbital Rashba textures: the case of Co/Al interfaces," (2025), arXiv:2503.16319 [cond-mat.mtrl-sci].
- ⁴²W. Wang, T. Wang, V. P. Amin, Y. Wang, A. Radhakrishnan, A. Davidson, S. R. Allen, T. J. Silva, H. Ohldag, D. Balzar, B. L. Zink, P. M. Haney, J. Q. Xiao, D. G. Cahill, V. O. Lorenz, and X. Fan, "Anomalous spin-orbit torques in magnetic single-layer films," *Nature Nanotechnology* **14**, 819–824 (2019).
- ⁴³D. Jo, D. Go, and H.-W. Lee, "Gigantic intrinsic orbital Hall effects in weakly spin-orbit coupled metals," *Phys. Rev. B* **98**, 214405 (2018).
- ⁴⁴L. Salemi and P. M. Oppeneer, "First-principles theory of intrinsic spin and orbital Hall and Nernst effects in metallic monoatomic crystals," *Phys. Rev. Mater.* **6**, 095001 (2022).
- ⁴⁵D. Go, H.-W. Lee, P. M. Oppeneer, S. Blügel, and Y. Mokrousov, "First-principles calculation of orbital Hall effect by Wannier interpolation: Role of orbital dependence of the anomalous position," *Phys. Rev. B* **109**, 174435 (2024).
- ⁴⁶A. Rothschild, N. Am-Shalom, N. Bernstein, M. Meron, T. David, B. Assouline, E. Frohlich, J. Xiao, B. Yan, and A. Capua, "Generation of spin currents by the orbital Hall effect in Cu and Al and their measurement by a Ferris-wheel ferromagnetic resonance technique at the wafer level," *Phys. Rev. B* **106**, 144415 (2022).
- ⁴⁷Y. Ben Tal, N. Am-Shalom, N. Bernstein, and A. Capua, "Measurement of the orbital Hall effect in Cu and Al by optically probed spin-torque- and microwave-ferromagnetic resonance," *Applied Physics Letters* **127**, 182405 (2025).
- ⁴⁸"The FLEUR project," <https://www.flapw.de/>.
- ⁴⁹D. Wortmann, G. Michalick, N. Baadji, M. Betzinger, G. Bihlmayer, J. Bröder, T. Burnus, J. Enkovaara, F. Freimuth, C. Friedrich, C.-R. Gerhorst, S. Granberg Cauchi, U. Grytsiuk, A. Hanke, J.-P. Hanke, M. Heide, S. Heinze, R. Hilgers, H. Janssen, D. A. Klüppelberg, R. Kovacik, P. Kurz, M. Lezaic, G. K. H. Madsen, Y. Mokrousov, A. Neukirchen, M. Redies, S. Rost, M. Schlipf, A. Schindlmayr, M. Winkelmann, and S. Blügel, "FLEUR," Zenodo (2023).
- ⁵⁰J. P. Perdew, K. Burke, and M. Ernzerhof, "Generalized Gradient Approximation Made Simple," *Phys. Rev. Lett.* **77**, 3865–3868 (1996).
- ⁵¹J. Chakraborty, K. Kumar, R. Ranjan, S. G. Chowdhury, and S. Singh, "Thickness-dependent fcc-hcp phase transformation in polycrystalline titanium thin films," *Acta Materialia* **59**, 2615–2623 (2011).
- ⁵²M. E. Straumanis and L. S. Yu, "Lattice parameters, densities, expansion coefficients and perfection of structure of Cu and of Cu-In α phase," *Acta Crystallographica Section A* **25**, 676–682 (1969).
- ⁵³C. Li, A. J. Freeman, H. J. F. Jansen, and C. L. Fu, "Magnetic anisotropy in low-dimensional ferromagnetic systems: Fe monolayers on Ag(001), Au(001), and Pd(001) substrates," *Phys. Rev. B* **42**, 5433–5442 (1990).
- ⁵⁴H. J. Monkhorst and J. D. Pack, "Special points for Brillouin-zone integrations," *Phys. Rev. B* **13**, 5188–5192 (1976).
- ⁵⁵G. Pizzi, V. Vitale, R. Arita, S. Blügel, F. Freimuth, G. Géranton, M. Gibertini, D. Gresch, C. Johnson, T. Koretsune, J. Ibañez-Azpiroz, H. Lee, J.-M. Lihm, D. Marchand, A. Marrazzo, Y. Mokrousov, J. I. Mustafa, Y. Nohara, Y. Nomura, L. Paulatto, S. Poncé, T. Ponweiser, J. Qiao, F. Thöle, S. S. Tsirkin, M. Wierzbowska, N. Marzari, D. Vanderbilt, I. Souza, A. A. Mostofi, and J. R. Yates, "Wannier90 as a community code: new features and applications," *J. Phys. Condens. Matter.* **32**, 165902 (2020).
- ⁵⁶F. Freimuth, Y. Mokrousov, D. Wortmann, S. Heinze, and S. Blügel, "Maximally localized Wannier functions within the FLAPW formalism," *Phys. Rev. B* **78**, 035120 (2008).
- ⁵⁷F. Freimuth, S. Blügel, and Y. Mokrousov, "Spin-orbit torques in Co/Pt(111) and Mn/W(001) magnetic bilayers from first principles," *Phys. Rev. B* **90**, 174423 (2014).
- ⁵⁸I. Lyalin and R. K. Kawakami, "Interface transparency to orbital current," *Phys. Rev. B* **110**, 104418 (2024).
- ⁵⁹M. Rang and P. J. Kelly, "Orbital relaxation length from first-principles scattering calculations," *Phys. Rev. B* **109**, 214427 (2024).
- ⁶⁰J. Sohn, J. M. Lee, and H.-W. Lee, "Dyakonov-Perel-like Orbital and Spin Relaxations in Centrosymmetric Systems," *Phys. Rev. Lett.* **132**, 246301 (2024).
- ⁶¹P. Tang and G. E. W. Bauer, "Role of disorder in the intrinsic orbital hall effect," *Phys. Rev. Lett.* **133**, 186302 (2024).
- ⁶²A. L. R. Barbosa, H.-W. Lee, and T. G. Rappoport, "Extrinsic orbital hall effect and orbital relaxation in mesoscopic devices," (2025), arXiv:2507.01941 [cond-mat.mes-hall].
- ⁶³T. Valet, H. Jaffrès, V. Cros, and R. Raimondi, "Quantum kinetic anatomy of electron angular momenta edge accumulation," (2025), arXiv:2507.06771 [cond-mat.mes-hall].
- ⁶⁴V. P. Amin, J. Li, M. D. Stiles, and P. M. Haney, "Intrinsic spin currents in ferromagnets," *Phys. Rev. B* **99**, 220405 (2019).
- ⁶⁵Q. Liu and L. Zhu, "Absence of orbital current torque in Ta/ferromagnet bilayers," *Nature Communications* **16**, 8660 (2025).
- ⁶⁶V. P. Amin, P. M. Haney, and M. D. Stiles, "Interfacial spin-orbit torques," *Journal of Applied Physics* **128**, 151101 (2020).
- ⁶⁷K.-W. Kim, B.-G. Park, and K.-J. Lee, "Spin current and spin-orbit torque induced by ferromagnets," *npj Spintronics* **2**, 8 (2024).
- ⁶⁸H. Hayashi, D. Go, S. Haku, Y. Mokrousov, and K. Ando, "Observation of orbital pumping," *Nature Electronics* **7**, 646–652 (2024).
- ⁶⁹T. Tanaka, H. Kontani, M. Naito, T. Naito, D. S. Hirashima, K. Yamada, and J. Inoue, "Intrinsic spin Hall effect and orbital Hall effect in *4d* and *5d* transition metals," *Phys. Rev. B* **77**, 165117 (2008).
- ⁷⁰H. Kontani, T. Tanaka, D. S. Hirashima, K. Yamada, and J. Inoue, "Giant Orbital Hall Effect in Transition Metals: Origin of Large Spin and Anomalous Hall Effects," *Phys. Rev. Lett.* **102**, 016601 (2009).
- ⁷¹J. L. Costa, E. Santos, J. B. S. Mendes, and A. Azevedo, "Revealing the Dominance of the Orbital Hall Effect over Spin in Transition Metal Heterostructures," (2025), arXiv:2506.08425 [cond-mat.mes-hall].
- ⁷²E. Santos, J. L. Costa, R. L. Rodriguez-Suarez, J. B. S. Mendes, and A. Azevedo, "Probing orbital currents through inverse orbital Hall and Rashba effects," (2025), arXiv:2510.05543 [cond-mat.mes-hall].
- ⁷³A. Pezo, D. García Ovalle, and A. Manchon, "Orbital Hall effect in crystals: Interatomic versus intra-atomic contributions," *Phys.*

- Rev. B **106**, 104414 (2022).
- ⁷⁴M. Rang and P. J. Kelly, “Orbital Hall effect in transition metals from first-principles scattering calculations,” *Phys. Rev. B* **111**, 125121 (2025).
- ⁷⁵R. B. Atencia, D. P. Arovas, and D. Culcer, “Intrinsic torque on the orbital angular momentum in an electric field,” *Phys. Rev. B* **110**, 035427 (2024).
- ⁷⁶H. Sun, A. Kazantsev, A. Principi, and G. Vignale, “Nonconserved density accumulations in orbital Hall transport: Insights from linear response theory,” *Phys. Rev. B* **111**, 075432 (2025).
- ⁷⁷R. W. Greening, D. A. Smith, Y. Lim, Z. Jiang, J. Barber, S. Dail, J. J. Heremans, and S. Emori, “Current-induced spin-orbit field in permalloy interfaced with ultrathin Ti and Cu,” *Applied Physics Letters* **116**, 052402 (2020).
- ⁷⁸S. Yakata, Y. Ando, T. Miyazaki, and S. Mizukami, “Temperature Dependences of Spin-Diffusion Lengths of Cu and Ru layers,” *Japanese Journal of Applied Physics* **45**, 3892 (2006).
- ⁷⁹N. Vijayan, D. Kumar, A. Du, L. Gao, Z. Xiao, H. I. Wang, R. Gupta, G. Jakob, S. Krishnia, Y. Mokrousov, and M. Kläui, “Observation of negative orbital torque from Vanadium,” (2025), arXiv:2508.16339 [cond-mat.mes-hall].